Soil & Tillage Research 124 (2012) 17–23

Contents lists available at SciVerse ScienceDirect

Soil & Tillage Research

journal homepage: www.elsevier.com/locate/still

# Effects of vegetation restoration on soil aggregate microstructure quantified with synchrotron-based micro-computed tomography

H. Zhou [a], X. Peng [a,*], S. Peth [b], T.Q. Xiao [c]

[a] State Key Laboratory of Soil and Sustainable Agriculture, Institute of Soil Science, Chinese Academy of Sciences, 71 East Beijing Road, Nanjing 210008, PR China
[b] Institute of Plant Nutrition and Soil Science, CAU Kiel, Olshausenstrasse 40, 24118 Kiel, Germany
[c] Shanghai Synchrotron Radiation Facility (SSRF), Shanghai Institute of Applied Physics, Chinese Academy of Sciences, Shanghai 201204, PR China

ARTICLE INFO

*Article history:*
Received 1 November 2011
Received in revised form 5 April 2012
Accepted 21 April 2012

*Keywords:*
Soil aggregate
Microstructure
Micro-computed tomography
Vegetation restoration
Multifractal

ABSTRACT

Vegetation restoration is expected to improve soil microstructure and therefore enhance soil stability and reduce soil erosion. The objective of this study was to evaluate the effect of long-term vegetation restoration on the modification of aggregate microstructure with synchrotron-based high resolution X-ray micro-computed tomography (SR-μCT). Triplicate aggregates (5-mm diameter) from (a) severely eroded bare land (BL) and (b) two decades of vegetation restoration land (RL) from Ultisol, Southern China, were collected and scanned with 9 μm voxel-resolution at SSRF (Shanghai Synchrotron Radiation Facility). ImageJ software and multifractal theory were used to analyze and quantify aggregate pore structure. Aggregate water stability, mechanical stability, and basic soil properties were also evaluated. Results showed that aggregate water stability and SOM content significantly increased in the RL treatment, while aggregate mechanical stability showed an inverse trend. The microstructure of aggregates had evolved from a very dense massive microstructure to a more porous hierarchical microstructure after two decades of vegetation restoration. Porosity, macro-porosity, fraction of elongated pores, and specific surface area were significantly higher in the RL aggregates as compared to the BL aggregates. Multifractal scaling was observed for the pore structure of the studied aggregates. Generalized dimensions ($D_q$) were significantly higher in the RL treatment as compared to BL treatment, indicating improved pore system after vegetation restoration. This improved microstructure of RL aggregates was attributed to the increased SOM that prompted soil aggregation. This study showed the positive effects of vegetation restoration on soil microstructure and water stability, which was beneficial to the reduction of soil erosion and to the improvement of soil quality in this region.



## 1. Introduction

Red soil, which covers about 1/5 of the land area of China, mostly distributes in the hilly areas of subtropical or tropical Southeast China. The intense agricultural use, together with the monsoon rainfall causes serious soil erosion in the red soil region (Zhao, 1992). In the severely eroded area, the A- and/or B-horizons were completely eroded and plinthic C-horizon exposed (Zhang et al., 2004). Counteracting the serious consequences of soil and water erosion, efforts have been undertaken to restore the eroded land since 1980s with vegetation restoration. Pioneer plants, for example *Lespedeza bicolor*, and other local species were chosen and planted in the eroded area.

Aggregate stability is regarded as one of the most important factors influencing soil erosion and soil quality (Barthès and Roose, 2002) and is therefore frequently examined (Le Bissonnais, 1996). Numerous methods have been proposed to measure aggregate stability under the effects of water, mechanical stress, and soil management (Kemper and Rosenau, 1986; Amézketa, 1999; Le Bissonnais, 1996). Some of them, for example Yoder method (Yoder, 1936) and Le Bissonnais method (Le Bissonnais, 1996), are easy to conduct and are widely used. However, the stability test cannot describe the status of aggregate structure or explain aggregation process (Young et al., 2001). The microstructure of soil aggregates determines soil stability as well as soil quality. By examining the microstructure of soil aggregates, aggregation status and process can be evaluated.

Direct investigation of soil aggregate structure used to rely on observation and quantification of soil thin sections or blocks using microscopy, electron microscopy and digital image analysis (Pagliai et al., 2004). These approaches provide detailed information on the fabric and constitution of soil aggregates but are time consuming and, more importantly, restricted to two-dimensional (2D) images. In recent years, the development of CT technique has offered a great opportunity to explore the three-dimensional (3D) inner space of soil aggregates non-destructively (Young et al.,

* Corresponding author. Tel.: +86 25 86881198; fax: +86 25 86881000.
*E-mail address:* xhpeng@issas.ac.cn (X. Peng).

0167-1987/$ – see front matter © 2012 Elsevier B.V. All rights reserved.
http://dx.doi.org/10.1016/j.still.2012.04.006

2001). However, it requires a high resolution (<10 μm) to capture the detailed information considering the size of soil aggregate (usually <10 mm in diameter). Micro-CT, especially SR-μCT, has the advantage of providing high resolution images with best signal to noise ratios and strong attenuation contrast at very fast scanning speed, and therefore is an excellent tool for studying soil aggregate microstructure (Wildenschild et al., 2002; Udawatta et al., 2008; Peth, 2010). For example, Peth et al. (2008) scanned soil aggregates with SR-μCT and found remarkable differences in aggregate morphology and quantitative pore parameters (e.g. porosity, pore size distribution, pore length, pore shape, etc.) between conventionally tilled plot and grassland plot.

Morphological parameters can depict partial soil pore characteristics, but cannot provide information regarding the spatial pattern of entire soil pore system (Baveye and Boast, 1998; Mooney and Korošak, 2009; Kravchenko et al., 2009; Vogel et al., 2010). Fractal and multifractal theory has been widely used to quantify soil structure in recent years (Bird et al., 2006). For a geometrical fractal object, its structure can be uniquely described by a fractal dimension ($D$), which is a non-integer value between 1 and 2 for the 2D object or between 2 and 3 for the 3D object (Baveye and Boast, 1998). However, more and more research illustrated that fractal dimension is insufficient to characterize the natural objects (Posadas et al., 2003). Fractal dimension only characterizes the overall spatial pattern of the studied objects but ignores the detailed inner structure (Posadas et al., 2003). On the other hand, multifractal analysis focuses on characterizing the inner structure variation by calculating the local densities of the studied objects (Evertsz and Mandelbrot, 1992). By extending the box-counting method to a cube-counting method, the mass fractal dimension of the 3D soil pore structure can be estimated (Perret et al., 2003; Gibson et al., 2006; Kravchenko et al., 2011). The application of multifractal theory on 3D soil structure, however, is very scare (Tarquis et al., 2009).

Our hypothesis in this study is that vegetation restoration improves soil aggregation, and hence changes soil microstructure, and increases pore complexity. Based on the long-term filed experiment and high resolution SR-μCT measurements, the objective of the study was to quantify and compare the 3D microstructure of soil aggregates from severely eroded bare land (BL) and Lespedeza restoration land (RL).

## 2. Materials and methods

### 2.1. Soils

The investigated site is located at the Ecological Experimental Station of Red Soil, Chinese Academy of Sciences in Yingtan, Jiangxi Province, China (116°5′30″E, 28°5′30″N). This region has a typical subtropical climate with a long term mean annual temperature of 17.7 °C and precipitation of 1706 mm. The red soil, developed from the kaolinitic Quaternary red clay, is classified as an Ultisol according to USDA soil taxonomy (Soil Survey Staff, 2003). The research area was severely eroded and gradually developed to bare land covered with an exposed plinthic layer. In 1987, Lespedeza shrum (*L. bicolor*) were transplanted to restore the eroded land and improve soil quality (Peng et al., 2003).

Soil samples were randomly collected with three replications from the surface layer (0–50 mm) of the BL and RL treatments using a shovel in June 2010 and carefully transported to the laboratory. Additionally, five undisturbed soil cores were used to determine the bulk density. Disturbed soil samples were air-dried at room temperature to about the plastic limit and then separated into aggregates by hand along natural failure surfaces. After further air-drying, a part of the sample was ground to pass a 2-mm sieve for particle size analysis and a 0.25-mm sieve for chemical analysis. Standard methods were used to determine chemical properties. Soil organic matter (SOM) was determined by oxidation with potassium dichromate in a heated oil bath. The total iron content was determined by AAS after digestion of the soil sample with a mixture of HF–$HNO_3$–$HClO_4$. Soil pH was measured using a glass electrode with a 1:2.5 soil:water ratio. Cation exchange capacity (CEC) was determined by the ammonium acetate method. Another aliquot of un-sieved samples was used to select 3–5 mm aggregates. The aggregates were stored in a desiccator before aggregate water stability and tensile strength measurement and SR-μCT scanning.

### 2.2. Aggregate water stability

Aggregate water stability was examined using the method proposed by Le Bissonnais (1996) and the fast wetting treatment was employed in this study. Five gram of dried aggregates was gently immersed in a 250 $cm^3$ beaker filled with 50 $cm^3$ deionized water. After 10 min, the water was removed by a pipette, and the aggregates were transferred to a 50 μm sieve which was immersed in ethanol. Then the 50 μm sieve was gently moved 5 times by hand to separate fragments <50 μm from those >50 μm. The >50 μm fraction was collected from the 50 μm sieve, oven-dried and gently dry-sieved by hand on a column of six sieves: 2000, 1000, 500, 200, 100 and 50 μm. The mass of each size fraction was measured and the <50 μm fraction was calculated by the difference between the total mass and the sum of the six classes. The aggregate stability was expressed by mean weight diameter (MWD), which is the sum the mass fraction of soil remaining on each sieve multiplied by the mean aperture of the adjacent mesh followed by

$$\mathrm{MWD} = \sum_{1}^{n+1} \frac{r_{i-1} + r_i}{2} \times m_i \quad (1)$$

where $r_i$ is aperture of the $i$th mesh (mm), $m_i$ is mass fraction of aggregates remaining on $i$th sieve and $n$ is number of the sieves.

### 2.3. Tensile strength of aggregates

Tensile strength of soil aggregates were determined by crushing test (Dexter and Kroesbergen, 1985) for evaluating aggregate mechanical stability. For each soil, 10 aggregates were selected randomly for tensile strength measurements. Point loads were applied with a loading frame (SANS CMT0104, Shenzhen, China) fitted with a 100 N load cell with a resolution accuracy of 0.001 N. The crosshead speed was 10 mm $min^{-1}$, and the force applied was recorded every 0.01 s. The maximum force, $F_{max}$ (N) was determined at the moment rupture starts and was used to calculate tensile strength, $T$ (kPa) by

$$T = 0.576 \times \frac{F_{max}/D^2}{1000} \quad (2)$$

where $D$ is the diameter of soil aggregate (m).

### 2.4. CT scanning and image analysis

Soil aggregates were scanned with a synchrotron-based μ-CT at beam line BL13W1 of the Shanghai Synchrotron Radiation facility (SSRF). Aggregates were fixed in a plastic tube that was mounted on a rotary stage. The stage rotated from 0° to 180° and absorption radiographs of the samples were acquired at the same step interval (about 0.1°). The filtered back-projection algorithm was used to reconstruct slices from the radiographs. About 430 slices with a size of 1200 × 1200 pixels for each slice were reconstructed for every sample. Every voxel represented a volume

of 9 μm × 9 μm × 9 μm, where the voxel associated attenuation coefficients were stored as grayscale values ranging from 0 (lowest attenuation) to 255 (highest attenuation). Due to the limitation of beam time, only three 3–5 mm aggregates were randomly selected from each soil for the SR-μCT study.

Images processing, visualization, and quantification were done with an open source software ImageJ ver. 1.44 (Rasband, 1997–2011). Ring artifacts in some slices were removed before image segmentation (Zhou et al., 2011). Examples of the grayscale slices are shown in Fig. 1. Segmentation of the grayscale slices was done by a global thresholding method and the threshold values were carefully chosen based on visual observation. To avoid edge effects, sub-volumes of the size of 360 × 360 × 360 voxels were extracted for further analyses representing an inscribed cube of the aggregate. Due to the resolution limit, only pores larger than 9 μm were recognized and studied. Volume rendering and visualization of the 3D aggregates were established with the ImageJ 3D viewer plugin (Schmid et al., 2010) and examples are shown in Fig. 1. The number-size information and the surface area of the 3D pore system were computed with the 3D Object Counter plugin (Bolte and Cordelières, 2006) for ImageJ. Pore sizes were expressed as the equivalent diameter. Pores were classified into 7 classes: <50, 50–100, 100–200, 200–300, 300–400, 400–500, and >500 μm, according to their equivalent diameters. Pore shape factor ($F$) was (Waddel, 1932).

$$F = \frac{A_e}{A}$$

where $A_e$ was the surface area of a sphere having a volume equal to that of the pore, $A$ is the measured pore surface area. The parameter $F$ equals 1 for a sphere, and smaller $F$ values refer to more irregular or elongated pore shapes. In this study, we classified pores to regular pores ($F \geq 0.5$), irregular pores ($0.2 < F < 0.5$), and elongated pores ($F \leq 0.2$) following Pagliai et al. (2004). The specific surface area was calculated as the total pore surface area divided by the volume of aggregates.

### 2.5. Multifractal analysis

Multifractal theory has been detailed in many studies (e.g. Feder, 1988; Evertsz and Mandelbrot, 1992). In this study, multifractal analysis was used to characterize pore system of soil aggregate with a range of generalized dimensions ($D_q$). The method of moments (MOM), which is based on a cube-counting method, is used in this study and a brief introduction is given below (Perrier et al., 2006).

The image stacks (i.e. 3D soil aggregate) are partitioned into $N_k$ cubes of side length $\delta_k$, for $\delta_k$ = 1, 2, 4, 8, 12, 20, 36, 40, 45, 60, 72, 90, 120, 180, and 360 voxels. The subscript $k$ stands for the stage of partition. For the $k$th partition, the probability density of pores of

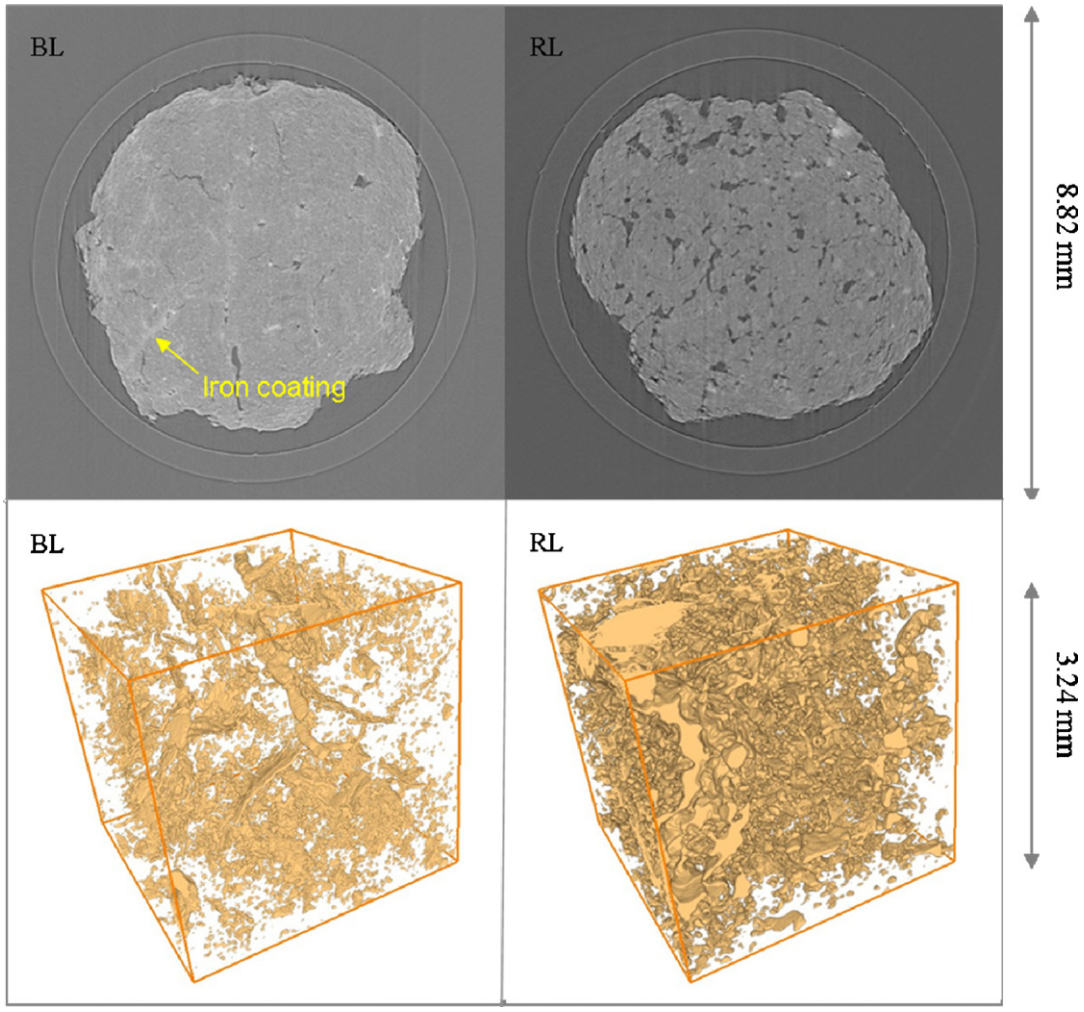


**Fig. 1.** Representative 2D slices (upper) and 3D pore structures (lower) of soil aggregate from the bare land and *Lespedeza* restoration land. *Note*: BL – bare land; RL – vegetation restoration land.

the $i$th cube, $\rho_i(\delta_k)$, is calculated as the total number of voxels representing pores within the cube divided by the total number of voxels representing pores of all the $N_k$ cubes. The partition function $\chi(q, \delta_k)$, which is a measure of the probability of pores, is calculated of order $q$:

$$\chi(q, \delta_k) = \sum_{i=1}^{N_k} (\rho_i(\delta_k))^q \quad (3)$$

where $q$ can theoretically be any real number. In this study $q$ was chosen between −10 and 10 in an increment of 1. For a multifractal field, this partition function scales with the cube size $\delta$ as

$$\chi(q, \delta) \propto \delta^{-\tau(q)} \quad (4)$$

where $\tau(q)$ is the mass exponent for order $q$. Hence, $\tau(q)$ can be estimated by linear regression of $\log(\chi(q,\delta))$ versus $\log(\delta)$ for any given value of $q$. The following relationship exists between $D_q$ and $\tau(q)$:

$$D_q = \frac{\tau(q)}{q-1} \quad (5)$$

For $q = 1$, $D_1$ is estimated directly from the slope of a linear regression analysis performed on: $\sum_{i=1}^{N_k} \rho_i(\delta) \log(\rho_i(\delta))$ versus $\log(\delta)$ (Perrier et al., 2006), which is identical to the calculation of information dimension. When $q = 0$ and 2, $D_0$ and $D_2$ are corresponding to capacity (mass) and correlation dimensions, respectively. The $D_q$ values are monotonically decreasing with increasing $q$ values.

### 2.6. Statistical analysis

To compare differences in porosity and multifractal parameters among the treatments, analysis of variance (ANOVA) was conducted using the GLM procedure in the SAS software program (SAS Institute, 1990). Mean values were tested using the least significant difference method (Duncan's LSD) at the $p = 0.05$ level of statistical significance.

## 3. Results

### 3.1. Soil properties

After the long-term vegetation restoration, many soil properties were changed considerably (Table 1). The RL soil texture became coarser than the initial BL soil. Clay content was reduced by 93 g kg$^{-1}$ while silt and sand fractions were increased. The bulk density was significantly ($P < 0.05$) deceased, while SOM content was increased significantly by 480% ($P < 0.001$). But, the total Fe content, CEC, and pH values showed no statistical significant difference between the two treatments ($P > 0.05$). Aggregate water stability (MWD) was also significantly ($P < 0.05$) higher in the RL treatment (1.65 mm) than in the BL treatment (1.50 mm). The mechanical stability, however, showed an inverse trend. The tensile strength of BL treatments was 1.45 times higher than that of RL treatments ($P < 0.05$).

**Table 1**
Basic properties of the aggregates from bare land and Lespedeza restoration land.

| | BL | RL |
|---|---|---|
| Sand (g kg$^{-1}$) | 173a | 236a |
| Silt (g kg$^{-1}$) | 286a | 316a |
| Clay (g kg$^{-1}$) | 541a | 448a |
| Bulk density (g cm$^{-3}$) | 1.38a | 1.19b |
| SOM (g kg$^{-1}$) | 3.25b | 15.6a |
| Fe (g kg$^{-1}$) | 51.7a | 49.9a |
| CEC (cmol kg$^{-1}$) | 15.8a | 16.2a |
| pH (1:2.5 $H_2O$) | 4.36a | 4.35a |
| MWD (mm) | 1.50b | 1.63a |
| Tensile strength (kPa) | 7.56a | 5.20b |

*Note*: BL – bare land; RL – vegetation restoration land; CEC – cation exchange capacity; SOM – soil organic matter; MWD – mean weight diameter. Values followed by a different letter within a row are significantly different at 0.05 level (LSD).

**Table 2**
General statistics for the pore systems of the aggregates from bare land and Lespedeza restoration land.

| | BL | RL |
|---|---|---|
| Porosity (%) | 1.78b | 12.68a |
| Total number of pores | 7200a | 6414a |
| Fraction of regular pore (%) | 13.1a | 4.35b |
| Fraction of irregular pore (%) | 41.8a | 13.8b |
| Fraction of elongated pore (%) | 45.1b | 81.9a |
| Mean shape factor | 0.64a | 0.51b |
| Specific surface area (mm$^{-1}$) | 2.74b | 7.62a |

*Note*: BL – bare land; RL – vegetation restoration land. Values followed by a different letter within a row are significantly different at 0.05 level (LSD).

### 3.2. Visualization of soil aggregates

Distinct microstructure morphologies were observed for aggregates from BL and RL treatments (Fig. 1). The BL aggregates had a denser massive microstructure with a few planes, channels and vughs. More porous microstructure with a large amount of vughs, and sub-angular smaller aggregates were observed for the RL aggregates. It is worth noting that regular high attenuation coefficients (lighter area) (Fig. 1) were observed along the pores of the BL aggregates, which were presumably related to the iron coatings because iron has a strong absorption of X-ray as pointed out by Peth (2010).

Discrepancy in the intra-aggregate pore structure of BL and RL was more evident in the 3D aggregate structure (Fig. 1). A large amount of inter-connected pores embedded in the RL aggregates formed a porous microstructure. In contrast, the BL aggregates had fewer pores, and most of which were disconnected. The plane pores in the BL aggregates were more evident in the 3D structure.

### 3.3. Quantification of pore structure

Quantitative information of the 3D pore system is listed in Table 2. The RL aggregates presented significantly higher porosity (>9 μm) but with less pore number than the BL aggregates did. The BL aggregates had a significantly greater fraction of regular and irregular pores as compared to the RL aggregates. On the contrast, the fraction of elongated pores, which is very important for soil water and gas transport, was 81.9% and 45.1% for the RL and BL aggregates, respectively. Compared to the BL aggregates, the RL aggregates had significantly greater specific surface area and lower mean shape factor.

Pore-size class distribution and corresponding cumulative pore-size distribution functions are shown in Fig. 2. The porosity with diameters larger than 50 μm was significantly higher in the RL aggregates as compared to the BL aggregates. The greatest difference was for the >500 μm pores accounting for more than 90% of the total porosity (>9 μm). However, the <50 μm porosity was nearly identical between the two treatments.

### 3.4. Generalized dimensions

In this study, the generalized dimensions were calculated using MOM. One critical step is to study the scaling relationship between partition function ($\chi(q,\delta)$) and scale size ($\delta$) to verify the multifractality of the structure. Linear behavior was found for

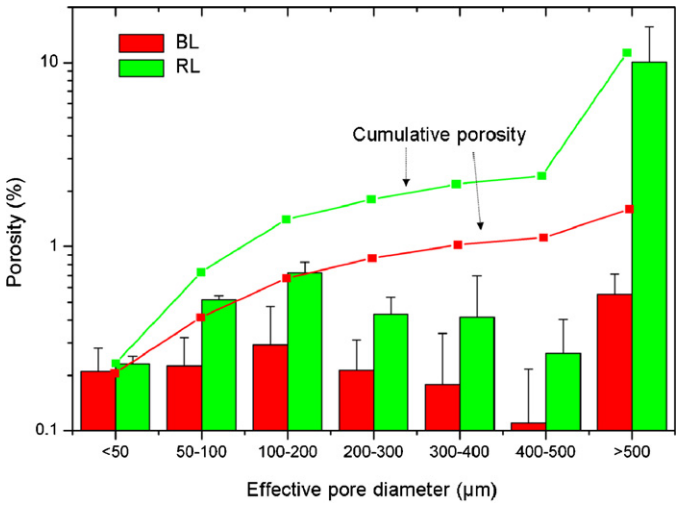


**Fig. 2.** Pore-size distributions and cumulative porosity for soil aggregates from the bare land and *Lespedeza* restoration land. *Note*: BL – bare land; RL – vegetation restoration land.

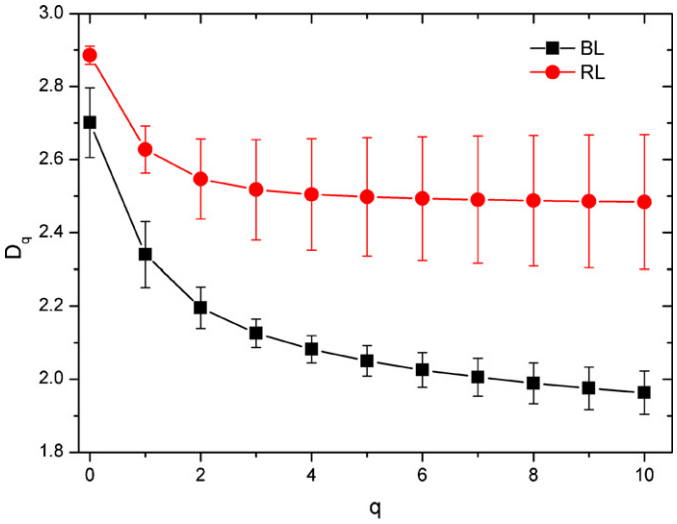


**Fig. 4.** Generalized dimensions ($D_q$) versus $q$, for the pore system of aggregates from bare land and *Lespedeza* restoration land. *Note*: BL – bare land; RL – vegetation restoration land. Error bars represent standard error.

the log-log plot between $\chi(q,\delta)$ versus $\delta$ within the studied scale for $q \leq 6$ (Fig. 3). This power-law scaling property in the linear range (right side of the vertical dashed line as shown in Fig. 3, i.e. >100 μm) indicated the existence of multifractality at this scale which was selected for further analysis. The coefficients of determination ($R^2$) for the estimation of $D_q$ were all >0.95.

Generalized dimensions ($D_q$) of the pore structure monotonically decreased with increasing $q$ values from 0 to 10 for both RL and BL aggregates (Fig. 4). The mass dimension ($D_0$) of the RL treatment was significantly higher than that of the BL treatment, suggesting improved space filling capacity of pore structure in the RL aggregates compared to BL aggregates. $D_1$, $D_2$ and other calculated generalized dimensions showed similar trends with $D_0$.

## 4. Discussion

Soil aggregate formation is the results of the interaction between aggregation and fragmentation processes elicited by abiotic or/and biotic (e.g. SOM, micro-organisms) factors (Bronick and Lal, 2005). Two decades after transplanting of *L. bicolor* onto the bare land, inputs of plant residues and roots decay from *L. bicolor* increased SOM as well as microbial activity (Zhang et al., 2010) considerably. They also decreased soil bulk density and increased aggregate water stability.

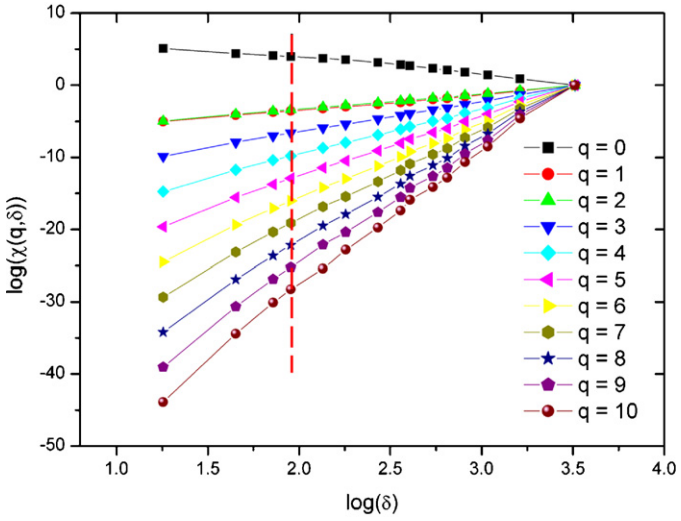


**Fig. 3.** Typical log-log plot of the partition function, $\chi(q,\delta)$ versus box size $\delta$ for the three-dimensional pore system of soil aggregate. *Note*: $q$ increases from 0 to +10 from top to bottom. The vertical dashed lines indicate the divisions between the two scaling regions.

Mechanisms of aggregation in the red soil region usually involve a variety of interactions of aggregation agents. Clay, SOM, and ferric oxides are important aggregation agents for the red soil in the subtropical region (Zhang and Horn, 2001). Many studies attributed the increased soil aggregation or stability to the increased SOM content (Zhang and Peng, 2006; Xie et al., 2008). In this study, the 4.8 times higher SOM content in the RL aggregates enhanced soil aggregation. The microstructure of soil aggregates developed from a very dense massive microstructure to a more porous microstructure which is qualitatively evident from visual observations as shown in Fig. 1. Quantitative analysis of the pore system (e.g. total porosity, macro-porosity, fraction of elongated pores, and specific surface area) also showed RL aggregates have more porous structure. Multifractal analysis found the aggregates had the multifractal scaling property and could be quantified by generalized dimensions. The $D_q$ values for the RL treatment were higher than those for the BL treatment, exhibiting a similar trend with porosity as reported by many researchers (Dathe et al., 2006; Udawatta et al., 2008; Luo and Lin, 2009; Kravchenko et al., 2011). The increased $D_q$ values suggested more complex pore structure in the RL aggregates as compared to BL aggregates (Kravchenko et al., 2011).

Another interesting result was observed from the tomography slices. Compared to the RL aggregates, more ferric oxides coatings (indicated by the high attenuation values and from direct observation of the samples under microscope) were observed along the channels or planes in the BL aggregates, although the total Fe contents were similar in both treatments (Table 1). This suggested that ferric oxides constituted the major Fe species in the BL aggregates. And they contributed more to soil aggregation in the BL treatment because of the very low SOM content (McIntyre, 1956; Markgraf and Horn, 2007). While in the RL treatment, few ferric oxides coatings were observed probably due to the formation of amorphous Fe–organic complexes (Lindsay, 1991; Oades and Waters, 1991) that decreased the Fe concentrations near the voids. The amorphous Fe–organic complexes were an efficient binding agent to increase soil aggregation (Barral et al., 1998), which resulted in higher aggregate water stability in the RL treatment as compared to BL treatment. However, this needs further investigations to prove it. However, detailed interaction mechanisms of iron, SOM, and

aggregation need more investigation using a combination of chemical, physical, and micromorphological methods.

Based on our results we suggest a conceptual model for aggregate development processes describing microstructural changes following land restoration. Initial aggregate microstructure from bare land soil is very dense with few macro-pores, while their shape observed is very well-defined planar and sharply angular. This is also widely agreed with many other researchers (Zhao, 1995; Zhang and Horn, 2001) who reported aggregates from plinthic layers (e.g. BL soil) to be similar to "pseudo stone" as said by local farmers. Main binding agent for aggregates of the plinthic layer in Ultisol is sesquioxide (Zhang and Horn, 2001; Barthès et al., 2008). This kind of aggregate represents a very strong resistance to mechanical stress but low stability to hydraulic stress as evidenced by high tensile strength but low aggregate water stability (Table 1). However, after a long-term enrichment of SOM, vegetation restoration improves aggregate water stability. This is partially thanks to the increase of water repellency as observed by Peng et al. (2003), which decreases entrapped air pressure and slaking stress. One the other hand, SOM bind sub-aggregates together, creating a porous microstructure from the initial massive microstructure. During this progress, the micro-organism played an important role (Zhang et al., 2010). The increase of porosity and specific surface area certainly reduces the contact point area between particles and aggregates (Horn et al., 1994; Dexter, 1988). It finally reduces tensile strength considerably ($P < 0.05$) as compared to initial bare land soil. The 2D and 3D soil aggregate morphology, together with quantitative analysis of the pore system, supported our hypothesis that vegetation restoration improved aggregate microstructure as compared to eroded bare land.

## 5. Conclusions

SR-μCT and accompanied digital image analysis can present 3D microstructure of soil aggregate with a high resolution. This provides an insight into the inner space of soil aggregates and the opportunity to investigate soil aggregation processes. Results showed that aggregate microstructure developed from a dense massive microstructure to a porous microstructure after two decades of vegetation restoration. Porosity, fraction of elongated pores, and specific surface area were significantly higher in the RL aggregates than in the BL aggregates. The SOM content and aggregate water stability was significantly higher in the vegetation restoration land as compared to the bare land but tensile strength was reduced. The improvement of aggregate structure and water stability was attributed to the enrichment of SOM that prompted soil aggregation in the RL treatment. Multifractal scaling was used to evaluating aggregate pore structure. The generalized dimensions ($D_q$), an index of pore structure complexity, showed more complicate aggregate microstructure in the RL than in the BL. This study provides a knowledge link between aggregate microstructure, aggregation and stability microstructure.

## Acknowledgements

This work was supported by National Natural Science Foundation of China (grant numbers 41101200 and 41171180), the National Key Technology R&D Program of China (2011BAD31B04), and the "100 Talents Program" of the Chinese Academy of Sciences. The authors thank SSRF (Shanghai Synchrotron Radiation facility) for supporting the use of the radiation source.

## References

Amézketa, E., 1999. Soil aggregate stability: A review. Journal of sustainable agriculture 14, 83–151.

Barral, M.T., Arias, M., Guerif, J., 1998. Effects of iron and organic matter on the porosity and structural stability of soil aggregates. Soil and Tillage Research 46, 261–272.

Barthès, B.G., Roose, E., 2002. Aggregate stability as an indicator of soil susceptibility to runoff and erosion; validation at several levels. Catena 47, 133–149.

Barthès, B.G., Kouakoua, E., Larré-Larrouy, M.C., Razafimbelo, T.M., de Luca, E.F., Azontonde, A., Neves, C.S.V.J., de Freitas, P.L., Feller, C.L., 2008. Texture and sesquioxide effects on water-stable aggregates and organic matter in some tropical soils. Geoderma 143, 14–25.

Baveye, P., Boast, C.W., 1998. Fractal geometry, fragmentation processes and the physics of scale-invariance: an introduction. In: Baveye, P., Parlange, J.Y., Stewart, B.A. (Eds.), Fractals in Soil Science. CRC Press, Boca Raton.

Bird, N., Diaz, M.C., Saa, A., Tarquis, A.M., 2006. Fractal and multifractal analysis of pore-scale images of soil. Journal of Hydrology 322, 211–219.

Bolte, S., Cordelières, F.P., 2006. A guided tour into subcellular colocalization analysis in light microscopy. Journal of Microscopy 224 (3), 213–232.

Bronick, C.J., Lal, R., 2005. Soil structure and management. A review. Geoderma 124, 3–22.

Dathe, A., Tarquis, A.M., Perrier, E., 2006. Multifractal analysis of the pore-and solid-phases in binary two-dimensional images of natural porous structures. Geoderma 134 (3–4), 318–326.

Dexter, A., Kroesbergen, B., 1985. Methodology for determination of tensile strength of soil aggregates. Journal of Agricultural Engineering Research 31, 139–147.

Dexter, A.R., 1988. Advances in characterization of soil structure. Soil and Tillage Research 11, 199–238.

Evertsz, C.J.G., Mandelbrot, B.B., 1992. Appendix B. Multifractal measures. In: Peitgen, H.-O., et al. (Eds.), Chaos and Fractals. New Frontiers of Science. Springer-Verlag, New York, pp. 921–953.

Feder, J., 1988. Fractals. Plenum Press, New York.

Gibson, J.R., Lin, H., Bruns, M.A., 2006. A comparison of fractal analytical methods on 2- and 3-dimensional computed tomographic scans of soil aggregates. Geoderma 134, 335–348.

Horn, R., Taubner, H., Wuttke, M., Baumgartl, T., 1994. Soil physical properties related to soil structure. Soil and Tillage Research 30, 187–216.

Kemper, W.D., Rosenau, R.C., 1986. Aggregate stability and size distribution. In: Methods of Soil Analysis, Part 1. Physical and Mineralogical Methods. Agronomy Monograph no. 9, Society of Agronomy/Soil Science Society of America, pp. 425–442.

Kravchenko, A.N., Wang, A.N.W., Smucker, A.J.M., Rivers, M.L., 2011. Long-term differences in tillage and land use affect intra-aggregate pore heterogeneity. Soil Science Society of America Journal 75 (5), 1658–1666.

Kravchenko, A.N., Martin, M.A., Smucker, A.J.M., Rivers, M.L., 2009. Limitations in determining multifractal spectra from pore-solid soil aggregate images. Vadose Zone Journal 8, 220–226.

Le Bissonnais, 1996. Aggregate stability and assessment of soil crustability and erodibility. I. Theory and methodology. European Journal of Soil Science 47, 425–437.

Lindsay, W.L., 1991. Iron oxide solubilization by organic matter and its effect on iron availability. Plant and Soil 130, 27–34.

Luo, L., Lin, H., 2009. Lacunarity and fractal analyses of soil macropores and preferential transport using micro-X-ray computed tomography. Vadose Zone Journal 8, 233–241.

Markgraf, W., Horn, R., 2007. Scanning electron microscopy-energy dispersive scan analyses and rheological investigations of South-Brazilian soils. Soil Science Society of America Journal 71, 851–859.

McIntyre, D.S., 1956. The effect of free ferric oxide on the structure of some terra rossa and rendzina soils. Journal of Soil Science 7, 302–306.

Mooney, S.J., Korošak, D., 2009. Using complex networks to model two- and three-dimensional soil porous architecture. Soil Science Society of America Journal 73, 1094–1100.

Oades, J.M., Waters, A.G., 1991. Aggregate hierarchy in soils. Australian Journal of Soil Research 29, 815–828.

Pagliai, M., Vignozzi, N., Pellegrini, S., 2004. Soil structure and the effect of management practices. Soil and Tillage Research 79, 131–143.

Peng, X., Zhang, B., Zhao, Q.G., Horn, R., Hallett, P.D., 2003. Influence of types of restorative vegetation on the wetting properties of aggregates in a severely degraded clayey Ultisol in subtropical China. Geoderma 115, 313–324.

Perret, J.S., Prasher, S.O., Kacimov, A.R., 2003. Mass fractal dimension of soil macropores using computed tomography: from the box-counting to the cube-counting algorithm. European Journal of Soil Science 54, 569–579.

Perrier, E., Tarquis, A.M., Dathe, A., 2006. A program for fractal and multifractal analysis of two-dimensional binary images: Computer algorithms versus mathematical theory. Geoderma 134 (3–4), 284–294.

Peth, S., 2010. Applications of microtomography in soils and sediments. In: Singh, B., Gräfe, M. (Eds.), Synchrotron-based Techniques in Soils and Sediments, vol. 34. Elsevier, Heidelberg, pp. 73–101.

Peth, S., Horn, R., Beckmann, F., Donath, T., Fischer, J., Smucker, A., 2008. Three-dimensional quantification of intra-aggregate pore-space features using synchrotron-radiation-based microtomography. Soil Science Society of America Journal 72, 897–907.

Posadas, A., Giménez, D., Quiroz, R., Protz, R., 2003. Multifractal characterization of soil pore systems. Soil Science Society of America Journal 67, 1361–1369.

Rasband, W.S., 1997–2011. ImageJ. U.S. National Institutes of Health, Bethesda, MD, USA. , http://imagej.nih.gov/ij/.

SAS Institute. 1990. SAS/STAT user's guide. vol. 2. Version sixth ed. SAS Inst., Cary, NC.

Schmid, B., Schindelin, J., Cardona, A., Longair, M., Heisenberg, M., 2010. A high-level 3D visualization API for Java and ImageJ. BMC Bioinformatics 11, 274.
Soil Survey Staff, 2003. Keys to Soil Taxonomy, Ninth ed. United States Department of Agriculture, Natural Resources Conservation Service, 332 pp.
Tarquis, A., Heck, R., Andina, D., Alvarez, A., Anton, J., 2009. Pore network complexity and thresholding of 3D soil images. Ecological Complexity 6, 230–239.
Udawatta, R.P., Anderson, S.H., Gantzer, C.J., Garrett, H.E., 2008. Influence of prairie restoration on CT-measured soil pore characteristics. Journal of Environment Quality 37, 219–228.
Vogel, H.J., Weller, U., Schlüter, S., 2010. Quantification of soil structure based on Minkowski functions. Computers Geosciences 36 (10), 1236–1245.
Waddel, H., 1932. Volume, shape, and roundness of rock particles. The Journal of Geology 40, 443–451.
Wildenschild, D., Vaz, C., Rivers, M., Rikard, D., Christensen, B., 2002. Using X-ray computed tomography in hydrology: systems, resolutions, and limitations. Journal of Hydrology 267, 285–297.
Xie, J., Yang, Y., Chen, G., Zhu, J., Zeng, H., Yang, Z., 2008. Effects of vegetation restoration on water stability and organic carbon distribution in aggregates of degraded red soil in subtropics of China. Acta Ecologica Sinica 28 (2), 702–709 (In Chinese).
Yoder, R.E., 1936. A direct method of aggregate analysis of soils and a study of the physical nature of erosion losses. Journal of the American Society of Agronomy 28, 337–351.
Young, I., Crawford, J., Rappoldt, C., 2001. New methods and models for characterising structural heterogeneity of soil. Soil and Tillage Research 61, 33–45.
Zhang, B., Deng, H., Wang, H., Yin, R., Hallett, P.D., Griffiths, B.S., Daniell, T.J., 2010. Does microbial habitat or community structure drive the functional stability of microbes to stresses following re-vegetation of a severely degraded soil? Soil Biology and Biochemistry 42, 850–859.
Zhang, B., Horn, R., 2001. Mechanisms of aggregate stabilization in Ultisols from subtropical China. Geoderma 99, 123–145.
Zhang, B., Peng, X., 2006. Organic matter enrichment and aggregate stabilization in a severely degraded Ultisol after reforestation. Pedosphere 16, 699–706.
Zhang, B., Yang, Y., Zepp, H., 2004. Effect of vegetation restoration on soil and water erosion and nutrient losses of a severely eroded clayey Plinthudult in southeastern China. Catena 57, 77–90.
Zhao, Q.G., 1995. On the problems of red soil degradation in China. Soils 27 (6), 281–285 (in Chinese).
Zhao, Q.G., 1992. Strategy and countermeasures in comprehensive utilization of agricultural resources in the Region of Red and Yellow Soils in China (in Chinese). In: Shi, H. (Ed.), Research on Red Soil Ecosystem. Sci. Press, Beijing (China), pp. 1–13.
Zhou, H., Peng, X., Zhang, Z., Wang, L., Xiao, T., Peng, G., 2011. Characterization of aggregate microstructure of paddy soils cultivated for different years with synchrotron based micro-CT. Transactions of the CSAE 27 (12), 343–347 (in Chinese).